communications biology

A Nature Portfolio journal

Article

https://doi.org/10.1038/s42003-025-08186-6

ATF1 and miR-27b-3p drive intervertebral disc degeneration through the PPARG/NF-κB signaling axis

Wei Guo[1,2,3] ✉, Kun Mu[4], Jing-Chao Geng[1], Hai-Yang Xing[1], Yu Dong[5], Wen-Dong Liu[1,3], Shuan-Chi Wang[1,2], Jia-Xiao Shi[1,2], Bao-Rui Xing[1,2,3], Jian-Yong Zhao[1,2,3] & Xiao-Ming Li[1,2,3] ✉

Intervertebral disc degeneration (IDD) is a primary cause of degenerative disc disease; however, the mechanisms underlying it remain unknown. Although great efforts have been made to develop new regenerative therapies, their clinical success is limited. Recent research has indicated that microRNAs (miRNAs) are significantly involved in the progression of IDD. Investigating the role of miRNA intervention in IDD could facilitate the development of therapeutic strategies based on miRNAs. However, circulating miRNAs have not yet been recognized as standard biomarkers for IDD. In this study, we observed that the expression of miR-27b-3p was elevated in the blood and nucleus pulposus (NP) tissue of patients with IDD. Furthermore, reducing the expression of miR-27b-3p was shown to impede the progression of IDD. MiR-27b-3p could reduce the expression of collagen II and ACAN and promote the expression of MMP13 and ADAMT-5 in vitro and in vivo. miR-27b-3p aggravated IDD progression by directly targeting peroxisome proliferator-activated receptor gamma (PPARG), a negative regulator of the NF-κB signal pathway. This study also established that PPARG serves a protective role in IDD. The overexpression of PPARG was able to mitigate the detrimental effects caused by miR-27b-3p in NP cells and animal models of IDD, indicating that miR-27b-3p facilitates the progression of IDD through its interaction with PPARG. Additionally, the transcription factor ATF1 was found to enhance the expression of miR-27b-3p by targeting its promoter region, thereby promoting the degenerative impact of miR-27b-3p on NP cells. Given that miR-27b-3p can promote IDD both in vitro and in vivo, it holds potential as a biomarker, and the inhibition of miR-27b-3p expression may represent a novel therapeutic target for IDD.

Intervertebral disc degeneration (IDD) is a prevalent spinal condition marked by the gradual reduction of disc space and sclerosis of the endplates[1]. This condition greatly reduces the life quality and places a considerable strain on healthcare systems worldwide[2]. The intervertebral disc (IVD) is composed of the nucleus pulposus (NP), situated centrally, and the annulus fibrosus (AF), which encircles it peripherally. The NP plays a critical role in regulating the balance of proteoglycans and collagen II within the extracellular matrix (ECM). IDD is characterized by the breakdown of proteoglycans and collagen II in the NP and results in diminished disk height and impaired biomechanical function[3]. Clinically, IDD manifests as spondylolisthesis, spinal stenosis, and disc herniation, all linked to persistent back pain and disability[4]. Therapeutically, IDD poses challenges due to its complex degenerative nature. Conservative and surgical interventions often provide limited long-term relief, addressing symptoms rather than underlying causes of IDD[4]. In recent years, with the development of gene therapy, approaches are available to prevent IDD progression at transcriptional and post-transcriptional stages[5,6]. Consequently, gaining a more comprehensive understanding of IDD is crucial for advancing the development of novel therapeutic strategies.

[1]Department of Orthopaedics, Hebei Province Cangzhou Hospital of Integrated Traditional Chinese Medicine-Western Medicine, Cangzhou, PR China. [2]Hebei Key Laboratory of Integrated Traditional and Western Medicine in Osteoarthrosis Research, Cangzhou, PR China. [3]Hebei Province Integrated Traditional Chinese and Western Medicine 3D Printing Technology Innovation Center, Cangzhou, PR China. [4]Department of Breast Surgery, Hebei Province Cangzhou Hospital of Integrated Traditional Chinese Medicine-Western Medicine, Cangzhou, PR China. [5]Department of Anaesthesiology, Hebei Province Cangzhou Hospital of Integrated Traditional Chinese Medicine-Western Medicine, Cangzhou, PR China. ✉e-mail: guow0319@163.com; lixiaomingcz@126.com

MicroRNAs (miRNAs) are endogenous noncoding RNAs that play crucial roles in skeletal pathophysiology[7]. Studies demonstrate that miRNAs inhibit the expression of target genes by interacting with their 3′ untranslated region (3′ UTR) [8]. miRNAs are integral regulators of essential cellular functions, including proliferation and apoptosis[9]. Notably, alterations in miRNA regulation have been linked to various degenerative diseases in humans[10,11]. Variations in miRNA expression patterns have been observed during the development of IDD[12]. Specifically, for example, miR-328-5p (upregulated), miR-583 (downregulated), and miR-141 (upregulated) have demonstrated significant upregulation or downregulation in IDD patients, highlighting their involvement in the regulation of genes associated with matrix degradation and inflammatory processes[13–15]. Blood, particularly circulating miRNAs, is the most frequently investigated clinical source for miRNA research. These miRNAs are found in human plasma/serum in a stable form, which makes them resistant to degradation and positions them as promising noninvasive biomarkers[16]. Despite their potential, circulating miRNAs have not yet been developed as standard clinical biomarkers for IDD. It is crucial to identify biomarkers that are causally linked to IDD. To address this gap, our study explores the causal relationships between miRNAs and IDD using two-sample Mendelian randomization methods. Given their role as key regulators of gene expression, miRNAs could provide valuable insights into the mechanisms underlying IDD development and may serve as specific biomarkers for assessing IDD severity and patient risk.

Dysregulation of transcription factors is associated with various diseases, including IDD, making them important targets for therapeutic intervention[17–19]. Therefore, understanding their mechanisms can provide insights into gene regulation and potential treatment strategies. However, the interplay between various transcription factors and their downstream targets is not fully understood. This complexity makes it challenging to delineate specific pathways involved in IDD. Previous research indicated that miRNAs are transcribed by RNA polymerase II, implying that the transcription of miRNAs is governed by mechanisms akin to those that control protein-coding genes[20]. While numerous transcription factors involved in miRNA expression have been recognized[21–24], the transcription factors that modulate miRNA expression in the context of IDD have yet to be investigated. Recently, Liu et al. discovered that the TP53/miR-183-5p/CCNB1 interaction network is correlated with IDD by bioinformatics research and qRT-PCR[25]. However, due to the lack of mechanistic investigation, this study did not clarify how this network leads to the occurrence of IDD.

This study investigates the possibility of using miRNAs as indicators for IDD by applying a two-sample Mendelian randomization method to evaluate the causal link between circulating miRNAs and the risk of IDD. By leveraging summary statistics derived from genome-wide association studies (GWAS), we identified multiple candidate miRNAs linked to IDD. Notably, we found that miR-27b-3p was significantly elevated in the blood and NP tissue samples of IDD patients compared to healthy controls. Our functional investigations indicated that miR-27b-3p promotes catabolic activity of NP cells through its targeting of the peroxisome proliferator-activated receptor gamma (PPARG) gene, a negative regulator of the NF-κB signaling pathway. We examined the specific effects of PPARG and the interactions between miR-27b-3p and PPARG on IDD phenotypes in vitro and in vivo. Additionally, we identified Activating Transcription Factor 1 (ATF1) as a regulator of miR-27b-3p expression and validated the interaction sites between ATF1 and the promoter region of miR-27b-3p. Subsequently, we assessed the synergistic effects of ATF1 and miR-27b-3p on the phenotype of degenerative NP cells. Our findings provide, strong evidence suggesting that miR-27b-3p could be an effective target for the prevention of IDD.

Results

MiRNAs associated with IDD risk

We employed the IVW method to identify and present all miRNAs significantly associated with IDD in Fig. 1, utilizing miRNA eQTL and IDD GWAS data. Our analysis revealed that four blood miRNAs were significantly linked to an increased risk of IDD, while three others were associated with a reduced risk. The most pronounced effect was noted for hsa-miR-27b-3p, where an increase of one standard deviation (SD) was associated with roughly an 8% rise in the likelihood of developing IDD. Comparable effects were also found for hsa-miR-139-5p and hsa-miR-152. Conversely, a one SD increase in hsa-miR-339-5p was linked to a 3% reduction in the odds of IDD, while hsa-miR-125b-5p showed a 2% decrease. Additionally, hsa-miR-125b-5p exhibited a similar protective effect against IDD.

The effect of miR-27b-3p on the degenerative phenotype and proliferation of human NP cells

To confirm the altered expression of miR-27b-3p, we conducted qRT-PCR on blood and nucleus pulposus (NP) tissues from 10 IDD patients and 10 healthy controls. The findings indicated that the levels of miR-27b-3p were significantly increased in both the blood and NP tissues of patients with IDD when compared to the control group. (Fig. 2A, C). Our findings also showed that the expression levels of miR-27b-3p were positively associated with the Pfirrmann grading of IDD. ($r = 0.870$, $p < 0.001$, $n = 20$, Fig. 2B). To investigate the role of miR-27b-3p in the development of IDD, we transfected human NP cells with either miR-27b-3p mimics or inhibitors and assessed changes in ECM components and proliferation. Immunofluorescence assays demonstrated that the suppression of miR-27b-3p led to an increase in the expression of extracellular matrix (ECM)-associated proteins, such as collagen II and aggrecan (ACAN). Conversely, the upregulation of miR-27b-3p significantly heightened the levels of matrix-degrading enzymes, including MMP-13 and ADAMTS-5. (Fig. 2D). Furthermore, our results also indicated that silencing miR-27b-3p significantly increased the expression of collagen II and ACAN mRNAs (Fig. 2E, F). Confirming our results at the protein level, overexpression of miR-27b-3p also led to a marked increase in mRNAs for MMP 13 and ADAMTS-5 (Fig. 2G, H). To assess the impact of miR-27b-3p on NP cell proliferation, we performed a CCK-8 assay. Over six time points (12 h, 24 h, 36 h, 48 h, 72 h, and 96 h), the miR-27b-3p inhibitor significantly facilitated NP cell proliferation, while the miR-27b-3p mimics notably suppressed it (Fig. 2I). Therefore, our findings suggest that increased level of miR-27b-3p inhibits matrix synthesis and reduces the proliferation of NP cells.

Intradiscal administration of a miR-27b-3p inhibitor mitigates the progression of IDD

To explore the therapeutic effects of miR-27b-3p in vivo, we administered local injections of the miR-27b-3p inhibitor (antagomir-27b-3p) in injury-induced IDD rat models on the first, seventh, and 14th days after surgery. Our findings indicated that the intradiscal delivery of the miR-27b-3p inhibitor notably reduced both cellular and structural degeneration of the AF and NP, as assessed by a modified histological grading system (Fig. 3A). This histological evidence suggests that silencing miR-27b-3p may have a therapeutic impact on the progression of IDD. Immunofluorescence analysis revealed that administering miR-27b-3p inhibitors down-regulated the expression levels of catabolic markers (MMP13 and ADAMT-5) and upregulated the expression levels of anabolic markers (collagen II and ACAN) in NP tissue (Fig. 3B). These findings suggest that miR-27b-3p plays a critical role in regulating the balance between degradation and synthesis in NP tissue. Consistent with these findings, qRT-PCR analysis confirmed a significant reduction in the mRNA levels of MMP13 and ADAMT-5 in the NP tissue of IDD rats treated with the miR-27b-3p inhibitor, alongside an increase in collagen II and ACAN mRNA levels (Fig. 3C–F).

Identification and verification of PPARG as a target of miR-27b-3p

After confirming the role of miR-27b-3p in IDD, we further explored its downstream mechanisms. TargetScanHuman, miRDB, miRTarBase, and StarBase were utilized to predict the target genes of the microRNAs and to examine the binding sites on the mRNA (Supplementary Data 1 in the Supplementary Data Excel file). All four databases indicated that

miRNA	N_SNPs	pval	OR (95% CI)
hsa–miR–27b–3p	3	0.0055	1.0782 (1.0224 – 1.1371)
hsa–miR–125b–5p	17	0.0175	0.9926 (0.9866 – 0.9987)
hsa–miR–139–5p	4	<0.001	1.0398 (1.0174 – 1.0628)
hsa–miR–152	7	<0.001	1.0515 (1.0315 – 1.0719)
hsa–miR–339–3p	7	0.0153	0.9777 (0.9601 – 0.9957)
hsa–miR–339–5p	6	0.0497	0.9809 (0.9622 – 1.0000)
hsa–miR–1270	8	0.0260	1.0051 (1.0006 – 1.0097)

0.8 1 1.2

Fig. 1 | Protective and harmful effects of miRNA on IDD. The square indicates the point estimate of OR, and the whisker shows its 95% confidence interval.

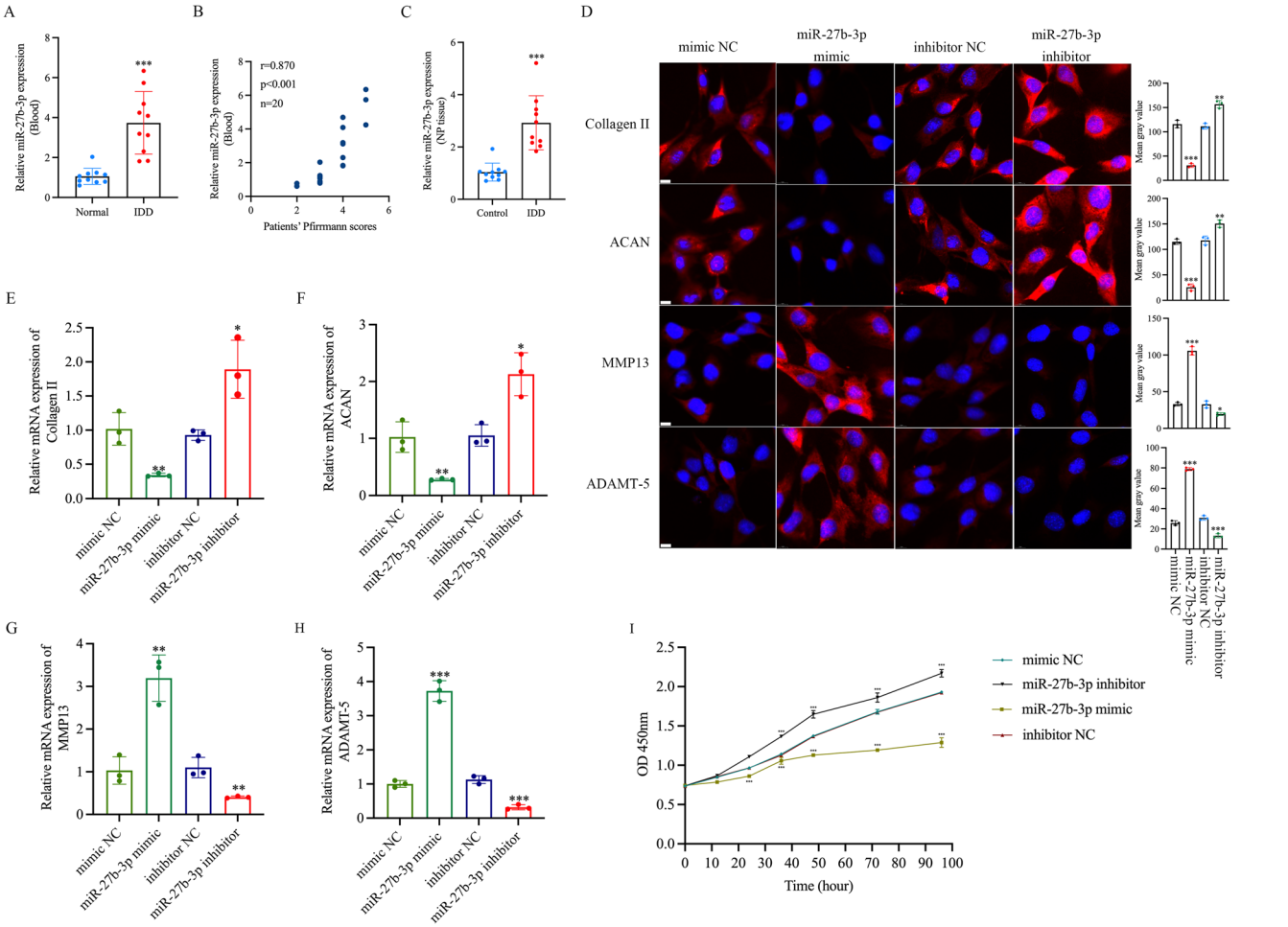

Fig. 2 | miR-27b-5p is upregulated in IDD patients and involved in the regulation of NP cell function. A The upregulation of miR-27b-3p in blood samples of IDD patients but not those of normal controls. $n = 10$, $^{***}P < 0.001$. **B** Correlation between miR-27b-3p expression and Pfirrmann grade of IDD ($n = 20$, r = 0.870, $P < 0.001$). **C** The upregulation of miR-27b-3p in NP tissue of IDD patients but not those of normal controls. $n = 10$, $^{***}P < 0.001$. **D** Immunofluorescence analysis of collagen II, ACAN, MMP13, and ADAMT-5 expression levels in human NP cells. The corresponding bar graphs show the quantitative analysis of each group (scale bar = 10 μm, magnification = 150×, $n = 3$, $^{**}P < 0.01$, $^{***}P < 0.001$). **E**–**H** The expression levels of collagen II, ACAN, MMP13, and ADAMTS-5 were detected by qRT-PCR. $n = 3$, $^{*}P < 0.05$, $^{**}P < 0.01$, $^{***}P < 0.001$. **I** Cell viability was assessed using a CCK-8 assay in each group. $n = 3$, $^{***}P < 0.001$.

thirteen genes (PPARG, RUNX1, CDH11, SEMA6A, WEE1, PLK2, CREB1, CCNG1, NR5A2, KHSRP, ADORA2B, EYA4, and PHB) were predicted (Fig. 4A). After mapping these genes to the STRING database, we found that seven genes exhibited significant interactions, with scores exceeding 0.7 (Fig. 4B). qRT-PCR analysis showed that overexpression of miR-27b-3p significantly reduced the mRNA levels of PPARG, RUNX1, and CREB1 (Fig. 4C). Notably, the expression levels of PPARG were found to be considerably reduced in the blood and NP tissues of patients with IDD when compared to those of healthy controls. (Fig. 4D, E). We subsequently performed fluorescence in situ hybridization (FISH) to investigate the distribution of miR-27b-3p and PPARG within NP cells. As expected, both miR-27b-3p and PPARG mRNA were found to co-localize in the same cytoplasmic region of NP cells (Fig. 4F). Additionally, levels of miR-27b-3p appeared elevated in degenerative NP cells, while those of PPARG appeared diminished (Fig. 4F).

To determine if miR-27b-3p interacts directly with the PPARG transcript, we executed a luciferase reporter assay. Two kinds of PPARG 3′UTR luciferase reporter vectors were created: one wild-type and one mutant-type (Fig. 4G). These vectors were cotransfected into NP cells along with miR-27b-3p mimics. As illustrated in Fig. 4H, the luciferase activity of the wild-type PPARG 3′UTR vector experienced a significant decrease due to the

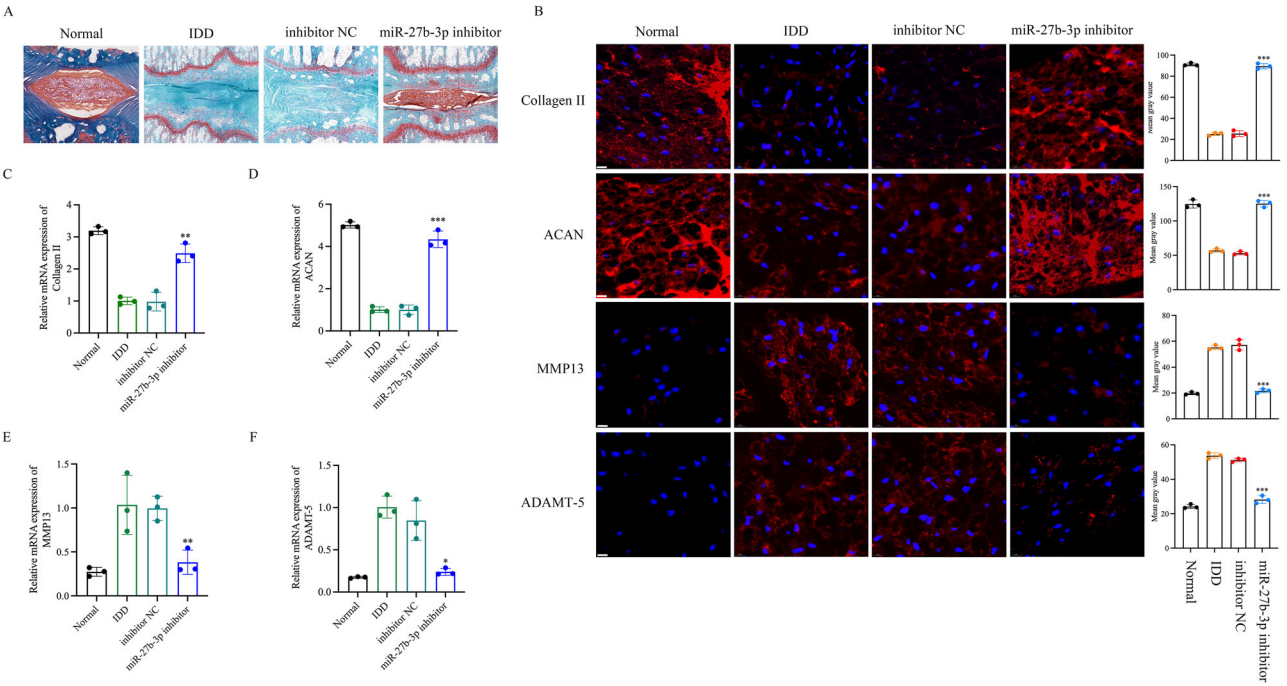

Fig. 3 | miR-27b-3p inhibitor suppresses progression of IDD. A Safranin-O/fast green staining of intervertebral discs in the indicated groups at 12 weeks after needle puncture. **B** Immunostaining for collagen-II, aggrecan, MMP-13, and ADAMTS-5 in the IDD rats model treated with miR-27b-3p inhibitors at 12 weeks after needle puncture. The corresponding bar graphs show the quantitative analysis of each group (scale bar = 10 μm, magnification = 120×, $n = 3$, $^{***}P < 0.001$). **C–F** The expression levels of collagen-II, aggrecan, MMP13, and ADAMTS-5 mRNA were detected by qRT-PCR. $n = 3$, $^{*}P < 0.05$, $^{**}P < 0.01$, $^{***}P < 0.001$. The data are shown as means ± standard deviations. NC negative control.

overexpression of miR-27b-3p. Our results indicate that miR-27b-3p inhibits the expression of PPARG mRNA by targeting its 3'UTR.

PPARG suppresses IDD-like phenotype in NP cells

Based on our identification of PPARG as a downstream target of miR-27b-3p, we examined the role of PPARG in NP cells. We found that overexpression of PPARG in NP cells produces similar effects as miR-27b-3p knockdown, enhancing the expression of collagen II and ACAN mRNA while suppressing the levels of MMP13 and ADAMT-5 mRNA (Fig. 5A–D). Conversely, the knockdown of PPARG led to decreased expression of collagen II and ACAN mRNA while increasing the levels of MMP13 and ADAMT-5 (Fig. 5A–D). Supporting these findings, immunofluorescence analysis revealed that PPARG reduced the levels of catabolic markers (MMP13 and ADAMT-5) and elevated the levels of anabolic markers (collagen II and ACAN) in NP cells at the protein level (Fig. 5E). Furthermore, a CCK-8 assay was performed to assess the influence of PPARG on the proliferation of NP cells. At multiple time intervals (12 h, 24 h, 36 h, 48 h, 72 h, and 96 h), it was observed that the overexpression of PPARG substantially promoted NP cell proliferation, while the knockdown of PPARG led to a marked decrease in proliferation (Fig. 5F). Previous research indicated that PPARG was a negative regulator of NF-κB signal pathway[26–28]. Thus, we proposed that PPARG might inhibit the NF-κB pathway's activation in NP cells, consequently slowing the advancement of IDD. Following TNF-α (an agonist of the NF-κB pathway) treatment, NP cells demonstrated a significant reduction in the expression of collagen II and ACAN, while levels of MMP13, ADAMT-5, and p-65 (which participates in the NF-κB pathway[29]) were increased in comparison to the control group (Fig. 5G). Notably, the overexpression of PPARG reversed the TNF-α induced decrease in collagen II and ACAN levels, as well as the increase in MMP13 and ADAMT-5 expression, along with the activation of the NF-κB pathway in NP cells (Fig. 5G). In conclusion, PPARG is crucial for preventing the degeneration of NP cells, likely through inhibiting the activation of the NF-κB pathway.

miR-27b-3p modulates IDD development through PPARG

Recognizing that miR-27b-3p directly interacts with PPARG, we subsequently explored the dynamic influences of both miR-27b-3p and PPARG on IDD. NP cells underwent co-transfection with miR-27b-3p and PPARG, followed by the evaluation of various related parameters. As depicted in Fig. 6A–E, miR-27b-3p resulted in an upregulation of MMP13 and ADAMT-5 at both mRNA and protein levels while concurrently reducing the levels of collagen II and ACAN. Notably, the overexpression of PPARG significantly alleviated the degenerative impacts of miR-27b-3p on NP cells. In terms of NP cell proliferation, the overexpression of miR-27b-3p resulted in a significant reduction in proliferation, which was notably reversed by the overexpression of PPARG (Fig. 6F). To further validate the in vivo effects of the miR-27b-3p/PPARG interaction on IDD, local injections were administered in rats. The intradiscal application of miR-27b-3p led to significant morphological degeneration of the intervertebral disc, while the overexpression of PPARG countered these effects (Fig. 6G). Additionally, in the intervertebral discs of rats, overexpression of miR-27b-3p increased the mRNA and protein levels of MMP13 and ADAMT-5 while inhibiting the expression of collagen II and ACAN (Fig. 6H–L). The overexpression of PPARG effectively counteracted the influence of miR-27b-3p on IDD-related mRNA and protein expression (Fig. 6H–L). Therefore, Our results indicate that the miR-27b-3p/PPARG axis contributes to the progression of IDD.

ATF1 is a transcription factor for miR-27b-3p

Using TransmiR (http://www.cuilab.cn/transmir), we identified a total of 142 predicted transcription factors that have the potential to regulate miRNA expression (Supplementary Data 2 in the Supplementary Data Excel file). In order to identify the IDD-related transcription factors, we performed differential expression analysis of GSE15227 datasets. There were 914 differentially expressed genes in IDD samples (Supplementary Data 3 in the Supplementary Data Excel file). Five intersection genes (NELFE, ATF1, NFYC, RUNX2, and TCF7L2) were obtained through the Venn diagram (Fig. 7A). The expression level change of these five

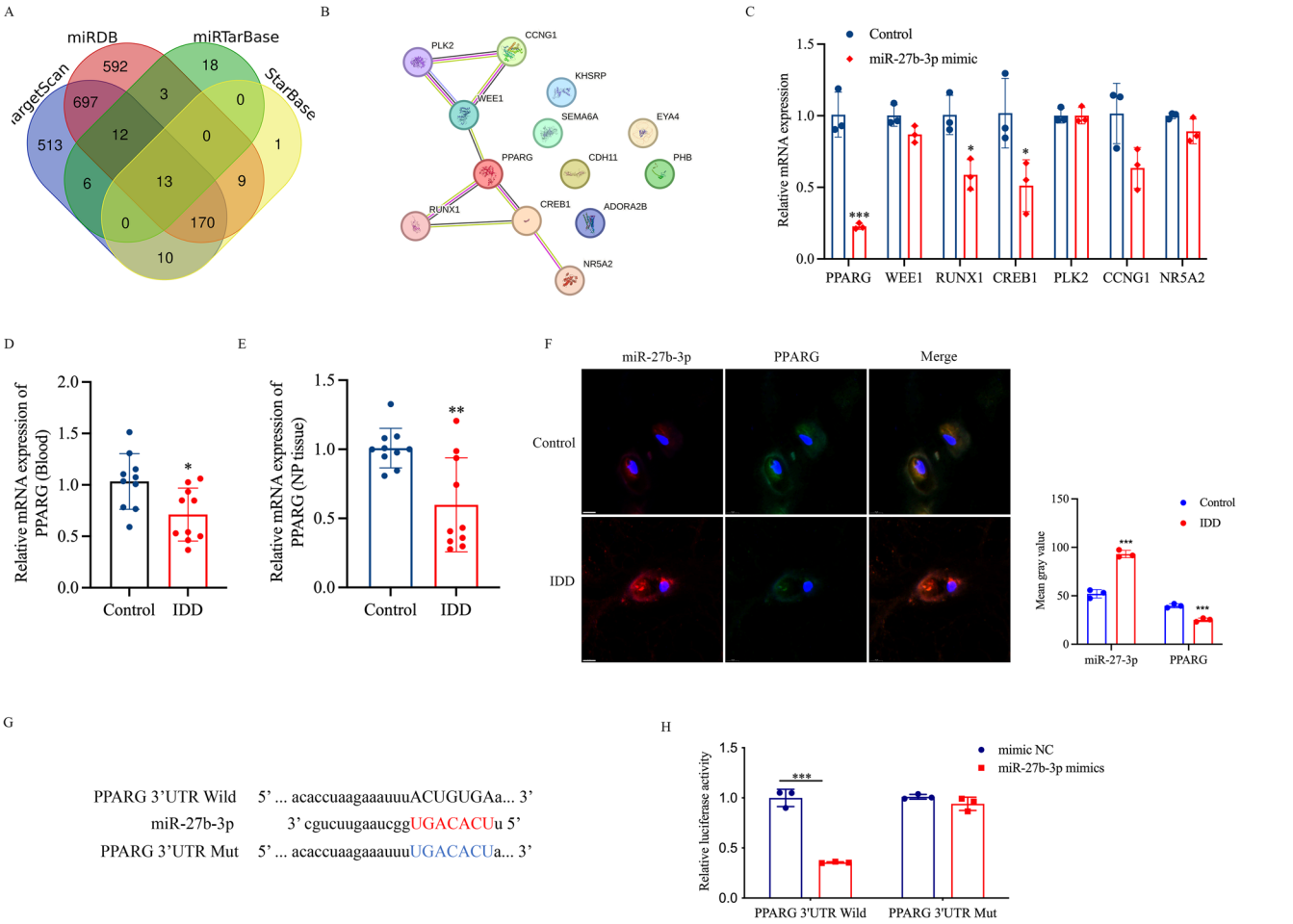

Fig. 4 | PPARG is a direct target gene of miR-27b-3p. A Venn diagram demonstrating the intersection of target genes predicted by different databases. **B** Thirteen genes identified from (**A**) were integrated into the STRING database, and a protein-protein interaction (PPI) network was constructed. **C** Analysis of the expression levels of predicted genes mRNA via qRT-PCR following transfection with miR-27b-3p mimics in human NP cells. $n = 3$, $^{*}P < 0.05$, $^{***}P < 0.001$. **D** The expression levels of PPARG in blood were measured in 10 IDD patients and 10 controls using qRT-PCR. $n = 10$, $^{*}P < 0.05$. **E** The expression levels of PPARG in NP tissues were measured in 10 IDD patients and 10 controls using qRT-PCR. $n = 10$, $^{**}P < 0.01$. **F** FISH detection of the subcellular localizations of miR-27b-3p and PPARG in NP cells (scale bar = 10 μm, magnification$n = 130\times$, $n = 3$, $^{***}P < 0.001$). **G** Sequence alignment of human miR-27b-3p and the 3′-UTR region of PPARG mRNA. Bottom, mutations in the 3′-UTR region of PPARG to create mutant luciferase reporter constructs. **H** Luciferase reporter assay in NP cells after co-transfection of PPARG luciferase constructs with miR-NC or miR-27b-3p mimics. $n = 3$, $^{***}P < 0.001$. The data are shown as means ± standard deviations.

genes is shown in Fig. 7B. Importantly, the expression of ATF1 was found to be markedly increased in the NP tissues of patients with IDD when compared to control samples (Fig. 7C). Consequently, we continued our investigation into the potential regulatory role of ATF1 on miR-27b-3p expression. Subsequently, NP cells were transfected with ATF1, and the expression levels of miR-27b-3p were assessed. Figure 7D showed that ATF1 overexpression significantly promoted miR-27b-3p expression, and knockdown of ATF1 expression markedly inhibited the expression of miR-27b-3p. Next, we further examined the effects of ATF1 on NP cells' degenerative phenotype. In NP cells, overexpression of ATF1 leads to a decrease in collagen II and ACAN mRNA expression while increasing the levels of MMP13 and ADAMT-5 mRNA. (Fig. 7E–H). Conversely, the knockdown of ATF1 resulted in elevated expression of collagen II and ACAN mRNA while reducing the levels of MMP13 and ADAMT-5 (Fig. 7E–H). Supporting these findings, immunofluorescence analysis revealed that ATF1 reduced the levels of anabolic markers (collagen II and ACAN) and elevated the levels of catabolic markers (MMP13 and ADAMT-5) in NP cells (Fig. 7I). Subsequently, NP cells were transfected with ATF1, either alone or in combination with miR-27b-3p inhibitors, and assessed for markers related to degeneration. As illustrated in Fig. 7J–M, the degenerative phenotype of NP cells triggered by ATF1 was notably counteracted by miR-27b-3p. Likewise, the inhibition of miR-27b-3p significantly reduced the detrimental effects of ATF1 overexpression on protein levels in NP cells (Fig. 7N).

ATF1 binds directly to the miR-27b-3p promoter to drive its expression

The transcription factor ATF1 is known to influence the expression of matrix metalloproteinases across multiple diseases[30,31]. According to analysis by TransmiR[32], there is a single ATF1 binding site located in the promoter region of miR-27b-3p. To determine whether ATF1 interacts directly with the promoter of miR-27b-3p, we cloned the complete 1 kb miR-27b-3p promoter (Fig. 8A) into a luciferase reporter plasmid. The 1 kb full-length reporter was cotransfected into NP cells with plasmids containing a vector, ATF1, or a mutant version of ATF1. The resulting luciferase activity showed a significant and positive response exclusively driven by ATF1 and not its mutated form (Fig. 8B). The complete reporter was segmented into three overlapping parts (P1, P2, and P3, Fig. 8A), with P1 containing a singular ATF1-binding motif, TGAGTCA. Data from the luciferase reporter assays demonstrate that the P1 segment interacts directly with ATF1 (Fig. 8C). Importantly, altering the ATF1-binding motif to the DraIII restriction site (CACXXXGTG) resulted in a reduction of ATF1-dependent transactivation (Fig. 8D). To verify the potential interaction

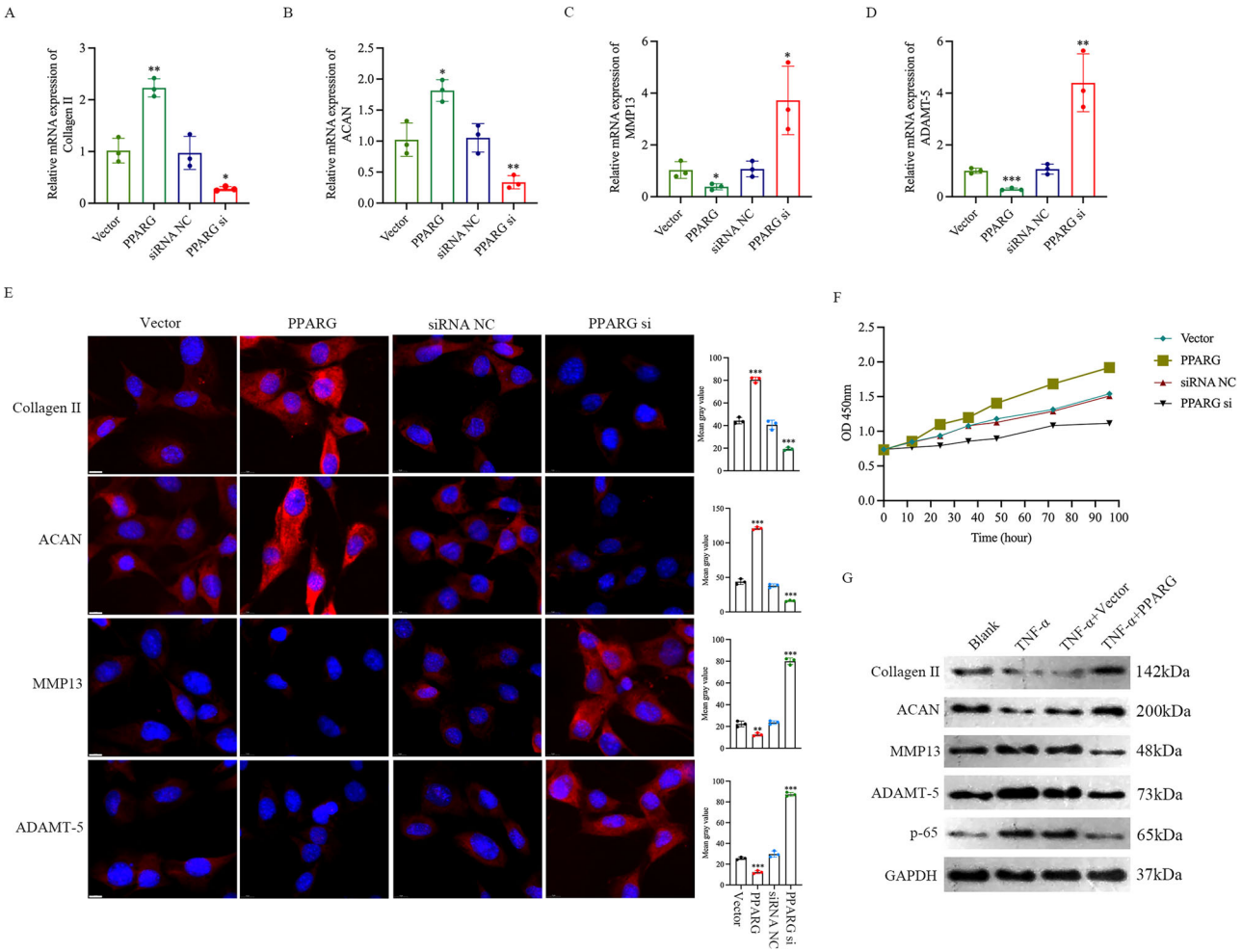

Fig. 5 | PPARG suppresses NP cell degenerative phenotype. A–D The expression levels of collagen II, ACAN, MMP13, and ADAMTS-5 in human NP cells were detected by qRT-PCR after transfection with the vector, PPARG, siRNA NC, or PPARG si plasmids. $n = 3$, $^{*}P < 0.05$, $^{**}P < 0.001$, $^{***}P < 0.001$.
E Immunofluorescence analysis of collagen II, ACAN, MMP13, and ADAMT-5 expression levels in human NP cells. The corresponding bar graphs show the quantitative analysis of each group (scale bar = 10 μm, magnification$n = 150\times$, $n = 3$, $^{**}P < 0.01$, $^{***}P < 0.001$). **F** Cell viability was assessed using a CCK-8 assay in each group. ($n = 3$). **G** The expression levels of the proteins collagen II, ACAN, MMP13, ADAMTS-5, and p65 in human NP cells treated with TNF-α and transfected with PPARG or blank vector, $n = 3$. The data are shown as means ± standard deviations.

between the P1 segment and ATF1, chromatin immunoprecipitation followed by quantitative PCR (ChIP–qPCR) was performed to analyze ATF1's genomic binding at the P1 region. Two qPCR probe sets were designed: one served as a negative control (NC probe) positioned 5 kb upstream of the transcription start site (TSS) of miR-27b-3p, while the other (p-miR-27b probe) encompassed the possible ATF1-binding motif within the P1 segment (Fig. 8E). The qPCR results from chromatin precipitated with ATF1 antibodies indicate a marked enrichment of ATF1 at the P1 region (Fig. 8F), supporting the hypothesis that ATF1 directly modulates the transcription of miR-27b-3p. In summary, the transcription factor ATF1 promotes the expression of miR-27b-3p, which subsequently affects the functions of miR-27b-3p related to the development of IDD (Fig. 8G).

Discussion

Despite the significant medical and societal costs associated with treating the various pathologies linked to IDD, there are limited clinical interventions available, and surgical options for symptomatic relief often yield suboptimal results. Moreover, the etiology and pathophysiology of IDD are still not fully elucidated. This lack of understanding has hindered the advancement of novel therapeutic strategies. In this study, we identified miR-27b-3p and explored the mechanisms through which miR-27b-3p contributes to IDD. Consistent with Mendelian randomization analysis of publicly available data, we observed significantly elevated levels of miR-27b-3p in degenerated human discs, an observation that was further confirmed through qRT-PCR in a separate cohort. Notably, a robust positive correlation was established between the expression levels of miR-27b-3p and the severity of IDD. The overexpression of miR-27b-3p led to a significant decrease in collagen II and ACAN expression while simultaneously enhancing the levels of MMP13 and ADAMTS-5. Consequently, these results indicate that miR-27b-3p may act as a potential biomarker for prognostic assessment in IDD and represent a novel target for therapeutic intervention. The present investigation revealed that the expression levels of PPARG were reduced in degenerated NP tissue and that miR-27b-3p is capable of directly binding to the 3' UTR of PPARG. The influence of miR-27b-3p on IDD was notably mitigated by the overexpression of PPARG. Furthermore, it was identified that the transcription factor ATF1 promotes the transcription of miR-27b-3p by engaging with its promoter region, thus enhancing its expression in NP cells. This study illustrated that ATF1 transcriptionally activates miR-27b-3p, leading to the inhibition of the downstream target PPARG and NF-κB signal pathway activation, which ultimately contributes to the decrease of collagen II and ACAN in NP and accelerates the progression of IDD. This newly identified pathway in NP cells may offer promising targets for therapeutic strategies in IDD.

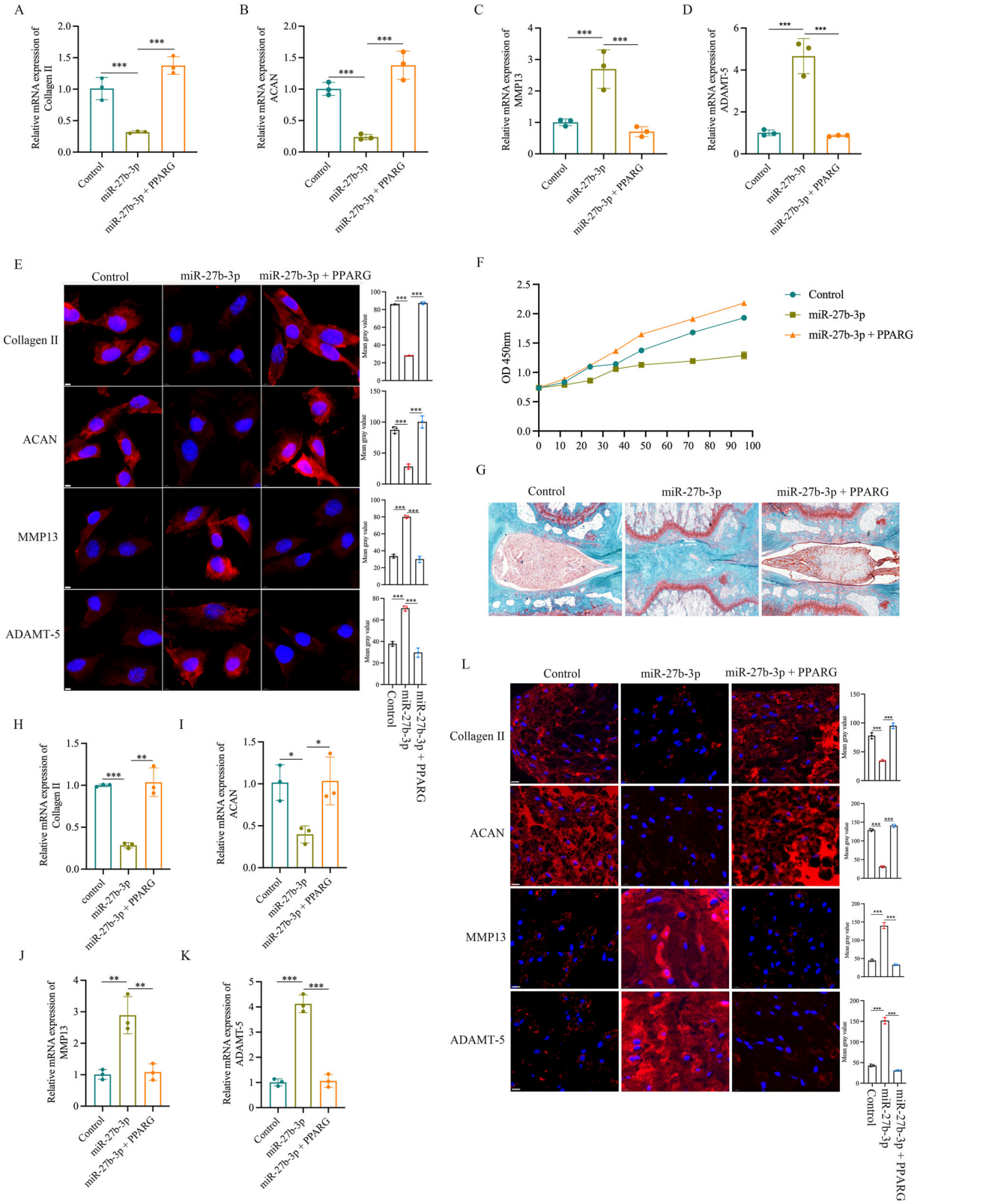

Fig. 6 | miR-27b-3p modulates IDD through PPARG. A–D Human NP cells were cotransfected with miR-27b-3p and PPARG, and qRT-PCT was examined for mRNA levels of collagen II, ACAN, MMP13, and ADAMT-5. $n = 3$, $^{***}P < 0.001$. **E** Human NP cells were cotransfected with miR-27b-3p and PPARG. Immunofluorescence analysis showed that PPARG overexpression blocked the effect of miR-27b-3p on Collagen-II, aggrecan, MMP13, and ADAMT5 expression. The corresponding bar graphs show the quantitative analysis of each group (scale bar = 5 μm, magnification = 160×, $n = 3$, $^{***}P < 0.001$). **F** Cell viability was assessed using a CCK-8 assay in each group. ($n = 3$). **G** Safranin-O/fast green staining of intervertebral discs in the indicated groups. **H–K** The expression levels of collagen-II, aggrecan, MMP13, and ADAMTS-5 mRNA of rat NP tissue were detected by qRT-PCR. $n = 3$, $^{**}P < 0.01$, $^{***}P < 0.001$. **L** Immunofluorescence analysis of collagen-II, aggrecan, MMP-13, and ADAMTS-5 in the indicated groups. The corresponding bar graphs show the quantitative analysis of each group (scale bar = 10 μm, magnification = 120×, $n = 3$, $^{***}P < 0.001$). The data are shown as means ± standard deviations.

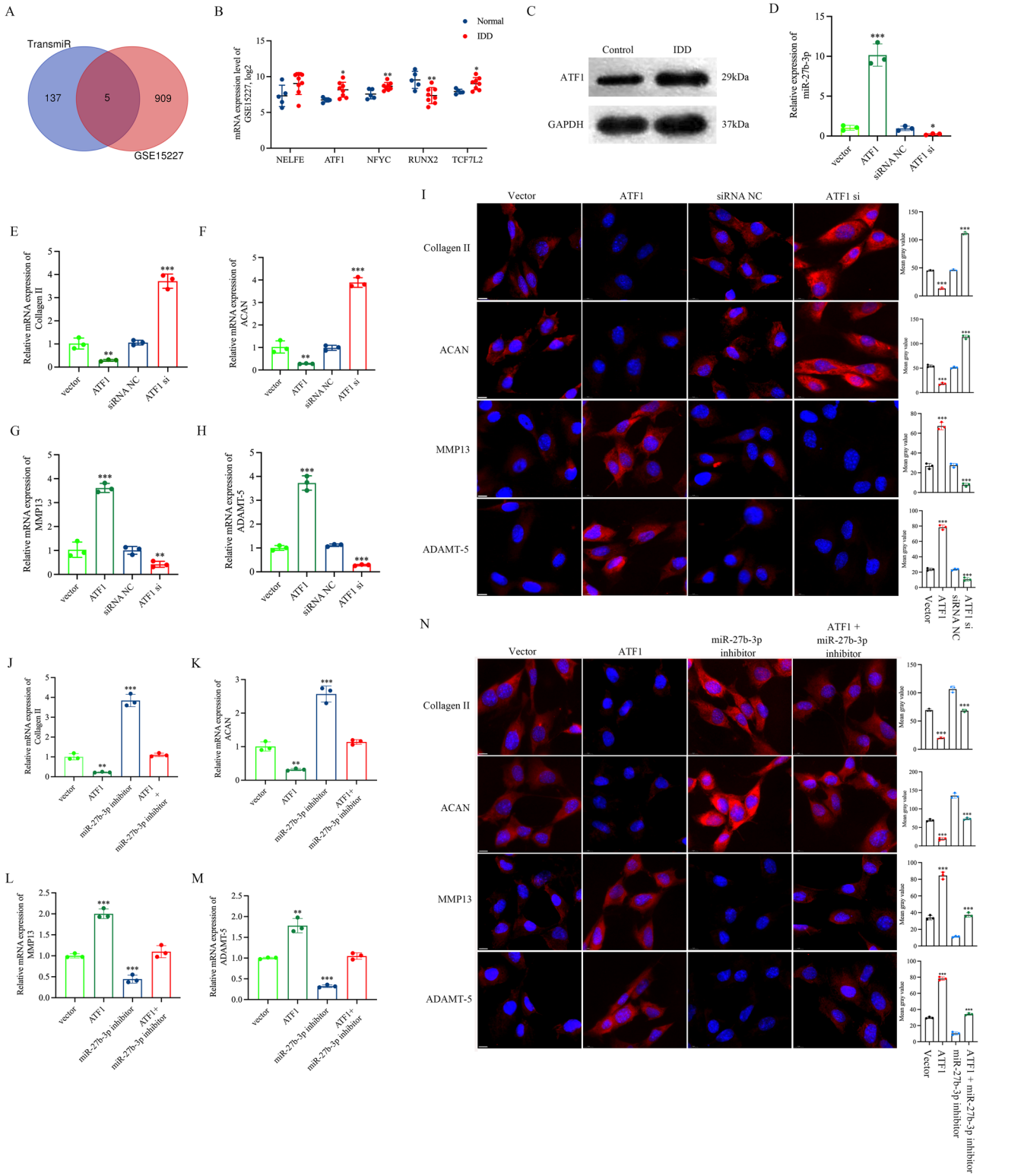

Fig. 7 | ATF1 regulates the expression of miR-27b-3p and influences NP cell degeneration via miR-27b-3p. A, **B** Venn diagram demonstrating the intersection of differential expression genes of the GSE15227 dataset and predicted transcription factors of miR-27b-3p and the expression level change of these five genes. **C** Western blot showing expression of ATF1 in IDD patients and normal controls. GAPDH is shown as a loading control. **D** Analysis of the expression levels of miR-27b-3p via qRT-PCR following transfection with ATF1 in human NP cells. $n = 3$, $^{*}P < 0.05$, $^{***}P < 0.001$. **E**–**H** The mRNA expression levels of collagen II, ACAN, MMP13, and ADAMTS-5 in human NP cells after ATF1 overexpression or knockdown. $n = 3$, $^{**}P < 0.01$, $^{***}P < 0.001$. **I** Immunofluorescence analysis of collagen-II, ACAN, MMP-13, and ADAMTS-5 in the indicated groups. The corresponding bar graphs show the quantitative analysis of each group (scale bar = 10 μm, magnification = 120×, $n = 3$, $^{***}P < 0.001$). **J**–**M** Human NP cells were cotransfected with ATF1 and miR-27b-3p inhibitor, and qRT-PCR was performed for mRNA levels of collagen II, ACAN, MMP13, and ADAMT-5. $n = 3$, $^{**}P < 0.01$, $^{***}P < 0.001$. **N** Immunofluorescence analysis showed that miR-27b-3p inhibitor blocked the effect of ATF1 on Collagen-II, aggrecan, MMP13, and ADAMT5 expression. The corresponding bar graphs show the quantitative analysis of each group (scale bar = 10 μm, magnification = 120×, $n = 3$, $^{***}P < 0.001$). The data are shown as means ± standard deviations.

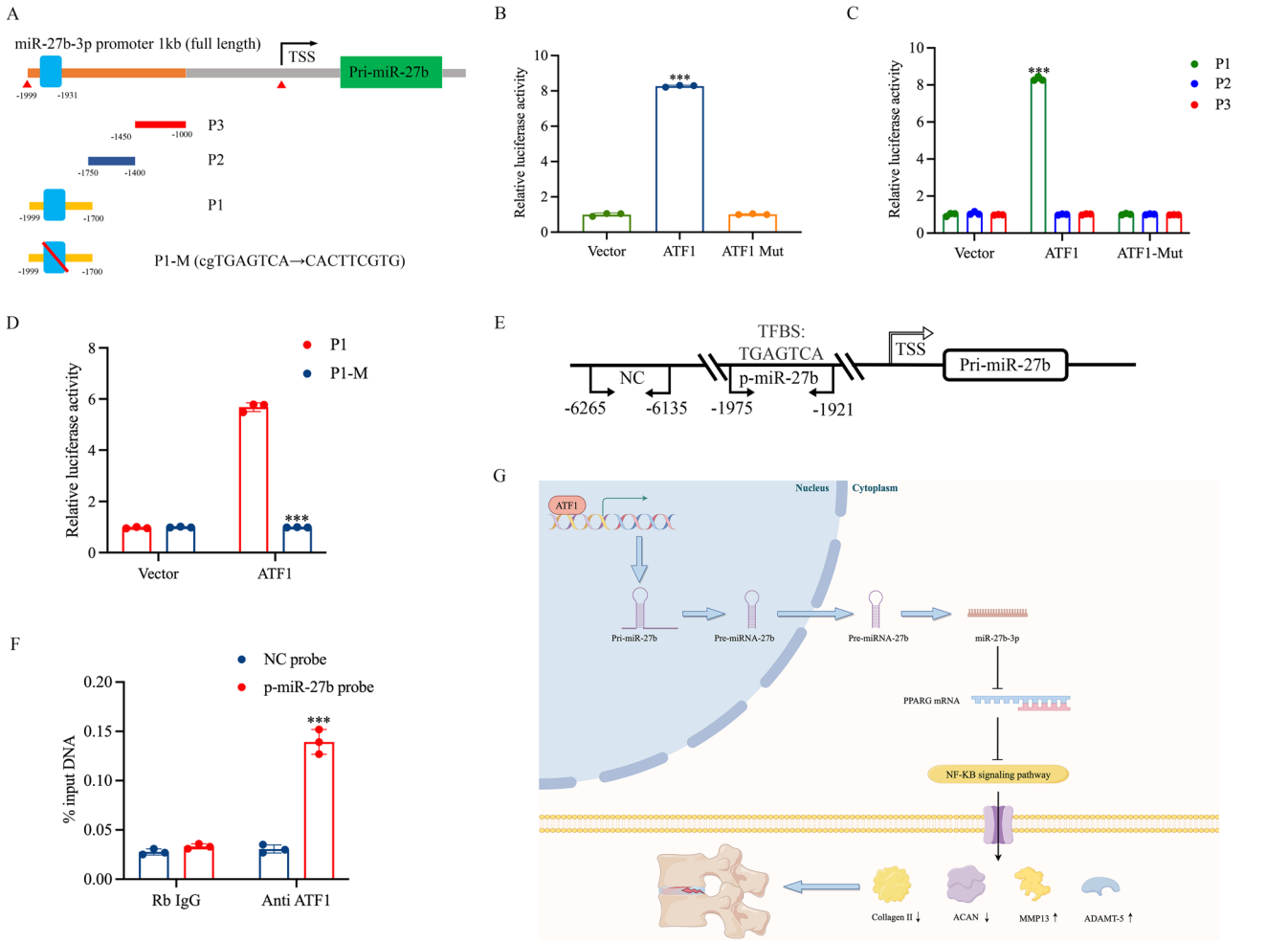

Fig. 8 | miR-27b-3p promoter reporters are transactivated by ATF1. A A diagram shows the relative positions of full-length and fragments of miR-27b-3p promoter reporters. **B**, **C** Responses of the full-length reporter and the individual fragments of the miR-27b-3p promoter to ATF1 or ATF1 mutant were investigated. $n = 3$, $^{***}P < 0.001$. **D** Reporter assays of the P1 fragment of the miR-27b-3p promoter containing a mutated ATF1-binding element as indicated. $n = 3$, $^{***}P < 0.001$. **E** A schematic illustrates the relative positions of qPCR probes to putative ATF1-binding elements for ChIP–qPCR experiments. **F** Antibody-pulled-down chromatins were analyzed by qPCR. $n = 3$, $^{***}P < 0.001$. **G** Schematic representation of the mechanisms by which miR-27b-3p mediates IDD development (By Figdraw, ID:ATIIT8af3c). Based on the findings described in the manuscript, ATF1 transcriptional activates miR-27b-3p expression and downregulates PPARG in NP cells, leading to the increase of p65. In turn, this leads to decreased collagen-II and aggrecan levels and increased levels of MMP-13 and ADAMTS-5, inducing an imbalance between the anabolic and catabolic activities of NP cells. These adverse factors initiate or accelerate IDD. The data are shown as means ± standard deviations.

ATF1 plays a crucial role in modulating cell survival and proliferation by functioning as either a transcriptional activator or repressor[33]. A wealth of research has identified associations between ATF1 can directly interact with the promoter regions of granzyme B (GzmB) and interferon-gamma (IFNγ), leading to diminished cytotoxic capabilities of T lymphocytes[34]. Silencing ATF1 resulted in the inhibition of migration and invasion in lung cancer cells[30]. ATF1 transcriptionally activates miR-214-5p expression, inhibiting the downstream target ITGA7, promoting osteoclast formation, and accelerating bone loss[24]. ATF1 can suppress the growth of cervical carcinoma cells through the regulation of miR-630[35]. Nonetheless, investigations into the role of ATF1 in IDD, particularly concerning its influence on miRNA expression, remain sparse. In the current study, we observed a significant increase in ATF1 expression in degenerative NP tissue, and the overexpression of ATF1 notably enhanced the degenerative phenotype of NP cells. Furthermore, our findings indicate that miR-27b-3p is a direct downstream target of ATF1 in NP cells, and we identified the interaction sites between these molecules, thereby enriching the understanding of ATF1's functionality. Four other intersecting genes were identified alongside ATF1 (NELFE, NFYC, RUNX2, and TCF7L2), and they should be investigated in future studies.

miRNAs play crucial roles in regulating various biological processes and have been implicated in IDD. A range of therapeutic strategies is currently under investigation, with cell therapies, endogenous repair mechanisms that activate intervertebral disc reparative cells, and treatments utilizing biological factors such as miRNAs emerging as the most promising options[36,37]. The impact of miR-27b-3p has been observed in several degenerative conditions. For example, miR-27b-3p has been shown to facilitate cardiac fibrosis, partly through the upregulation of profibrotic ECM genes in atrial fibroblasts[38]. Tavallaee et al. reported elevated expression levels of miR-27b-3p in the synovium of patients with knee osteoarthritis and in mice subjected to destabilization of the medial meniscus, which induced arthritis. Furthermore, the administration of a miR-27b-3p mimic into mouse knee joints led to a phenotype resembling synovial fibrosis, marked by increased synovitis scores and elevated expression of COL1A1 and α-smooth muscle actin[39]. However, the role of miR-27b-3p in IDD remains poorly understood. Our research offers a fresh perspective on the potential clinical application of miR-27b-3p as both a diagnostic marker and a therapeutic target for IDD. The heightened expression of miR-27b-3p in patients with IDD suggests its utility as a reliable biomarker for this prevalent musculoskeletal disorder. Our in vitro and in vivo findings

indicate that inhibiting miR-27b-3p protects intervertebral discs from the characteristic pathological changes associated with IDD by promoting the expression of ECM proteins (Col II and Aggrecan), suppressing the expression of ECM-degrading enzymes (MMP13 and ADAMT-5), and enhancing the proliferation of NP cells. Consequently, these results support the potential of miR-27b-3p as a direct therapeutic target for reversing the progression of IDD.

PPARG, an important member of the nuclear receptor superfamily, consists of an amino-terminal activation domain, a central DNA binding domain, and a carboxy-terminal ligand binding domain[40]. This receptor is involved in numerous biological functions, particularly in the regulation of metabolism and the modulation of inflammatory responses. A decrease in PPARG levels can lead to heightened inflammation and immune activity[41]. Hsieh et al. illustrated that PPARG agonists can suppress the expression of MMPs in macrophages during inflammatory processes[42]. Previous research indicated that an increase in PPARG expression can mitigate inflammation, while its inhibition raises the levels of pro-inflammatory cytokines, such as TNF-α, IL-6, and IL-1β, in serum[43]. Beyond its anti-inflammatory roles, PPARG is also implicated in the regulation of cell growth and apoptosis[44]. Liu et al. demonstrated that PPARG enhances the resistance of nucleus pulposus (NP) cells to oxidative stress and inhibits the expression of MMP3, MMP13, and ADAMT-5 induced by tert-butyl hydroperoxide[45]. The PPARG agonist pioglitazone has been shown to reduce neuropathic pain by decreasing the accumulation of reactive oxygen species (ROS) in dorsal root ganglion neurons[46]. Excessive ROS are well-known contributors to oxidative stress and have been frequently observed in the microenvironments of degenerative intervertebral discs. Prior studies have shown that ROS can lead to the loss of NP cells or diminish their functionality, resulting in an imbalance between the anabolic and catabolic processes of the extracellular matrix (ECM), which is characteristic of IDD[47]. In our investigation, we demonstrated that the downregulation of PPARG in NP cells resulted in a reduction in collagen II and ACAN expression while simultaneously increasing the levels of MMP13 and ADAMT-5, together with the evidence that ROS accumulation is an important stimulatory for NF-κB signal activation[47–49]. We suggest that low PPARG expression leads to ROS accumulation in NP cells, which activates the NF-κB signal pathway and promotes the development of IDD. Furthermore, our findings revealed that PPARG is a target gene of miR-27b-3p. The overexpression of PPARG was shown to counteract the effects of miR-27b-3p-induced IDD in both cellular and animal models. However, this study did not delve into the specific mechanisms through which PPARG influences NP cell degeneration. Further research is necessary to explore the role of PPARG in maintaining intervertebral disc homeostasis.

Jiang et al.[50] showed that miR-338-3p was associated with IDD, but miR-338-3p was not identified as being associated with IDD in the present study. On the other hand, the present study identified other miRNAs associated with IDD but with a lower strength than miR-27b-3p. Those miRNAs have different targets and mechanisms in IDD that will warrant additional investigation.

In this research, we discovered that ATF1 facilitates the progression of IDD by regulating the miR-27b-3p/PPARG pathway, thereby elucidating a potential mechanism for the involvement of miR-27b-3p in IDD development. These results not only deepen our comprehension of the molecular underpinnings of IDD but also offer new insights into the potential for clinical diagnosis and therapeutic strategies. Notably, the expression levels of miR-27b-3p could function as biomarkers for individuals with IDD, assisting clinicians in making more precise decisions regarding early diagnosis and treatment planning. Moreover, targeted interventions aimed at the ATF1/miR-27b-3p/PPARG pathways may present novel therapeutic avenues for patients suffering from IDD. Further investigations are warranted to confirm these results in larger cohorts and to assess the potential clinical implications of these molecular targets.

Materials and methods

Ethics statement

Approval for this study was granted by the ethics committees of the Cangzhou Hospital of Integrated Traditional and Western Medicine in Hebei Province. Human nucleus pulposus (NP) tissue samples were collected from patients who underwent surgical procedures at the same institution. All patients provided written informed consent for the utilization of their tissue specimens in research activities.

Clinical samples

According to the Pfirrmann classification, intervertebral discs were categorized as normal if they were graded 3 or lower (white disc), while IDD was identified when at least one intervertebral disc was graded 4 or higher (black disc) based on MRI T2-weighted imaging. Degenerative NP specimens and blood samples were collected from 10 patients with IDD who underwent discectomy. Normal samples were sourced from 10 patients with fresh traumatic vertebral fractures, matched for age and sex, who required decompressive surgery due to neurological deficits. All IDD cases were clinically diagnosed by two experienced spine surgeons through physical examinations and MRI assessments.

MiRNA eQTL data and IDD GWAS data

MicroRNA expression quantitative trait loci (eQTLs) are genome-wide assessments that identify genetic variants linked to the expression levels of microRNAs[51]. In this investigation, miRNA eQTL data were sourced from a prior population-based study involving 5329 participants. Whole blood samples from these individuals were subjected to quantitative reverse transcription PCR (qRT-PCR) to quantify the levels of miRNA expression. To reduce the likelihood of false-positive findings, a Benjamini–Hochberg adjusted false discovery rate (FDR) threshold of 0.1 was implemented, which corresponds to a raw p-value of 1×10^{-5}. The analysis was specifically focused on cis-miRNA-eQTLs, which are defined as single nucleotide polymorphisms (SNPs) situated within 1 MB of either side of the corresponding miRNA.

Summary statistics data about IDD were sourced from the FinnGen consortium, comprising 37,636 cases and 270,964 controls. Comprehensive details regarding these datasets and consortia are outlined in Supplementary Table 2. In order to ensure the robustness of our analytical approach, stringent quality control measures were implemented for SNPs. This process involved excluding non-biallelic single nucleotide polymorphisms (SNPs); SNPs with ambiguous alleles; missing rsID; duplicated rsID or genomic positions; absent from the 1000 Genomes Project phase 3; exhibiting discrepancies in genomic coordinates or alleles compared to the 1000 Genomes Project phase 3; and all SNPs located on chromosomes X and Y.

Mendelian randomization analysis

Inverse variance-weighted (IVW) was chosen as the primary method for Mendelian randomization (MR) analysis. Estimates from IVW were derived by evaluating Wald ratios for all genetic variants based on the premise that there is no horizontal pleiotropy among the single nucleotide polymorphisms (SNPs). FDR was utilized to mitigate potential type I errors with a value less than 0.05 for IDD. Supplementary analyses were also performed using multiple MR methods to ensure the reliability of our findings. The study utilized the weighted median method to address potential violations of the assumption of IVW analysis, allowing for the presence of up to half of the instrumental variables being invalid. We utilized the MR-Egger regression method to identify and adjust for pleiotropic effects, where genetic variants influence both the exposure and the outcome.

Injury-induced IDD model and therapeutic experiment

The rat model of IDD induced by injury was established through the needle puncture method. In brief, after administering general anesthesia to 12-week-old Sprague-Dawley rats, the coccygeal discs at the Co6/Co7 levels were accessed and punctured with a 21-G syringe needle, which penetrated

from the AF to the NP. The needle was maintained at a depth of 5 mm in the intervertebral disc for 10 s. The neighboring Co7/Co8 disc levels remained unpunctured and were utilized as control segments.

Twenty male rats that had previously undergone the injury-induced IDD procedure were randomly divided into three groups (n = 5 each): Group 1 (healthy rats, no interventions), Group 2 (Control: IDD model), Group 3 (Inhibitor NC: IDD model with antagomir-control), and Group 4 (miR-27b-3p inhibitor: IDD model with antagomir-27b-3p). The antagomir-27b-3p, and their corresponding controls were obtained from RiboBio (RiboBio Co., Guangzhou, China). The rats received injections of 10 μl of a solution containing either the antagomir-27b-3p or the negative controls on days 1, 7, and 14 following the needle puncture. Disc samples were collected at two time points: the 6th week and the 12th week following the intervention.

The recombinant adenovirus was constructed by amplifying the PPARG sequence from human genomic DNA through PCR, which was subsequently inserted into the pDC311-U6-MCMV-EGFP vector (Hanbio Co. Ltd, Shanghai, China). Additionally, PPARG siRNA was procured from Life Technologies. A total of 15 IDD model rats were included in this research and assigned to three groups randomly (n = 5 each). Three and 7 days after the injection of agomir-27b-3p in the IDD model, the intervertebral discs received injections of either PPARG (1×10^{-9} viral particles) or the vector control (1×10^{-9} viral particles). The rats were euthanized using an overdose of pentobarbital 8 weeks following the adenovirus injection.

The experimentation protocol (CZX2022090) was approved by the ethics committee of Hebei Province Cangzhou Hospital of Integrated Traditional and Western Medicine, and all procedures were performed in compliance with established guidelines. We have complied with all relevant ethical regulations for animal use.

Cell cultures

Primary NP cell obtained from patients who underwent discectomy. Human NP tissues were sectioned into 1 mm^3 fragments and subjected to two washes with a solution of 10% fetal bovine serum in phosphate-buffered saline (PBS) (Gibco, NY, USA). Following this, the tissues were incubated in Dulbecco's Modified Eagle Medium (DMEM) (Gibco, NY, USA). The NP cells were subsequently resuspended and cultured in DMEM that was enriched with 1% penicillin-streptomycin and 10% fetal bovine serum (FBS). The incubation was carried out at 37 °C within a 5% CO_2 environment. Upon reaching confluence, the cells were detached from the culture surface using trypsin and were then subcultured at a dilution ratio of 1:3. The cells were used in the third passage.

Quantitative real-time polymerase chain reaction (qRT-PCR)

Total RNA was isolated utilizing TRIzol (Invitrogen Life Technologies, CA, USA). The RNA samples underwent conversion to complementary DNA (cDNA) with the iScripts cDNA Synthesis Kit (Quanta BioSciences, MD, USA), using GAPDH as the normalization reference. The extracted microRNA was quantified with the qScript microRNA cDNA Synthesis Kit (Quanta BioSciences, MD, USA), employing U6 small nuclear RNA (snRNA) as the internal control. Quantitative reverse transcription PCR (qRT-PCR) was conducted using a SYBR Green Real-Time PCR Kit (Quanta BioSciences), and gene expression levels were determined through the comparative threshold cycle method (ΔΔCt). The primer sequences utilized in the experiments are listed in Supplementary Table 1.

Immunofluorescence

Fix cells/tissues with 4% paraformaldehyde (PFA) at room temperature for 15 min, wash with PBS (3 × 5 min), and permeabilize with 0.3% Triton X-100 for 10 min at room temperature. After PBS washing, block samples with 5% BSA or species-matched normal serum for 1 h at room temperature to minimize nonspecific binding. Incubate with primary antibody diluted in blocking buffer at 4° C overnight or 2 h at room temperature, followed by washing with PBS-T (0.1% Tween-20, 3 × 5 min). Apply fluorophore-conjugated secondary antibody (Alexa Fluor 594, 1:500) and incubate in the dark for 1 h at RT, then wash with PBS-T (3 × 5 min). Stain nuclei with DAPI (1 μg/mL) for 5 min, rinse with PBS, mount with antifade medium, and image using a fluorescence microscope with appropriate filters. The primary antibodies used in the experiments included Collagen II (Abcam ab34712, 1:100), Aggrecan (Abcam ab3778, 1:100), MMP13 (Abcam ab39012, 1:100), and ADAMT-5 (Abcam ab246975, 1:100).

miR-27b-3p, PPARG and ATF1 transfection

To induce overexpression or silencing of miR-27b-3p, human NP cells were subjected to transfection with either miR-27b-3p mimics, inhibitors, or their corresponding negative controls (a randomly sequenced miRNA mimic molecule that has been extensively tested in human cell lines and tissues to have no detectable effect on known miRNA functions) (Cat. No: 4464060 and 4464078, Life Technologies) utilizing Lipofectamine RNAiMAX Transfection Reagent (Invitrogen). For the purpose of downregulating PPARG expression, human NP cells were transiently transfected with either PPARG siRNA or a control siRNA (Cat. No: 143093 and 4457292, Thermo Fisher Scientific), employing Lipofectamine 3000 Transfection Reagent (Invitrogen). Similarly, to inhibit ATF1 expression, human NP cells underwent transient transfection with either ATF1 siRNA or control siRNA (Cat. No: 115614 and 4457292, Thermo Fisher Scientific).

Luciferase constructs and reporter assay

Fragments of the PPARG mRNA 3′ UTR, comprising wild-type (wild) and mutant (mut) miR-27b-3p binding sites, were cloned into the psiCHECK-2 luciferase reporter vector (Promega, WI, USA). The constructs, in conjunction with either an miR-27b-3p expression plasmid or a control plasmid, were cotransfected into human NP cells alongside the wild-type or mutant PPARG 3′ UTR and their respective control plasmids. Luciferase assays were performed utilizing the Dual-Glo Luciferase Assay System (Promega, WI, USA), with luciferase activity measured using a fluorescence microplate reader (BioTek, USA).

To confirm the interaction between ATF1 and the miR-27b promoter, DNA fragments containing the predicted binding site or a mutated binding site were cloned downstream of the Renilla psiCHECK-2 vector. NP cells were subsequently cotransfected with the luciferase reporter vectors and either the pcDNA3.1-ATF1 overexpression vector or the ATF1 homeodomain deletion mutant (ATF1-Mut). After 48 h, luciferase activity was evaluated using the Dual-Glo Luciferase Assay System (Promega, WI, USA). The miR-27b promoter region (−1000 to −1999, relative to the transcription start site) was PCR amplified from human genomic DNA and inserted into the luciferase reporter psiCHECK-2. Additionally, three shorter promoter fragments (P1, P2, and P3) and mutant-binding site fragments (P1-M) were generated through PCR from the miR-27b promoter.

Cell counting kit-8 (CCK-8) assay

Cell proliferation was evaluated using the CCK-8 assay kit according to the manufacturer's instructions. Human NP cells, which were transfected with various constructs including miR-27b-3p mimics, control mimics, miR-27b-3p inhibitors, control inhibitors, PPARG, PPARG siRNA, or control siRNA, were plated into 96-well plates and incubated for durations of 12, 24, 36, 48, 72, and 96 h. Following this incubation, CCK-8 was introduced to the cells, and they were allowed to incubate for an additional 3 h. The absorbance was subsequently measured at a wavelength of 450 nm.

Fluorescence in situ hybridization (FISH)

The subcellular localization of miR-27b-3p and PPARG was detected by FISH, following the protocol outlined by a previous study[52]. The experimental procedure is as follows: Begin with sample preparation by fixing cells/tissues with 4% paraformaldehyde (PFA) at room temperature for 15 min, followed by PBS washing (3 × 5 min) and permeabilization with 0.1% Triton X-100 for 10 min. For probe preparation, mix fluorescently labeled probes with hybridization buffer (containing formamide and

dextran sulfate) to a final concentration of 10 ng/μL, denature at 75 °C for 5 min, and immediately chill on ice for 2 min. Apply denatured probes to samples, cover with a coverslip, and hybridize in a preheated humidified chamber at 37 °C for 8 h in the dark. Post-hybridization washes are performed sequentially with 2 × SSC and 0.1 × SSC buffers at 42 °C (2 × 10 min each) to remove nonspecific binding. Counterstain nuclei with DAPI (1 μg/mL) for 5 min, rinse with PBS, and mount with antifade medium. Visualize signals using a fluorescence microscope with appropriate filters, and analyze images using ImageJ. The probe designed for miR-27b-3p was tagged with Cy5, whereas the probe specific for PPARG was tagged with Alexa Fluor® 488 (Thermo Fisher Scientific, Waltham, MA).

Western blotting

Protein concentrations were quantified using the Micro BCA Protein Assay Kit (Thermo Fisher Scientific, 23235) with bovine serum albumin standards. Equal amounts of protein lysates (20 μg per lane) were denatured in Laemmli buffer (62.5 mM Tris-HCl pH 6.8, 2% SDS, 10% glycerol, 0.01% bromophenol blue) containing 5% β-mercaptoethanol at 95 °C for 5 min. Samples were resolved on 10% SDS-polyacrylamide gels through electrophoresis at 80 V for 30 min followed by 120 V for 1 h in Tris-glycine running buffer (25 mM Tris, 192 mM glycine, 0.1% SDS).

Proteins were transferred to 0.45 μm PVDF membranes (Bio-Rad, 1620177) using wet transfer at 100 V for 90 min in Towbin buffer (25 mM Tris, 192 mM glycine, 20% methanol). Membranes were blocked with 5% non-fat milk in TBST (20 mM Tris-HCl pH 7.6, 150 mM NaCl, 0.1% Tween-20) for 1 h at room temperature, then incubated overnight at 4 °C with the following primary antibodies diluted in blocking buffer: Rabbit anti-Collagen II (Abcam ab34712, 1:1000), Rabbit anti-Aggrecan (Abcam ab3778, 1:1000), Rabbit anti-MMP13 (Abcam ab39012, 1:3000), and Rabbit anti-ADAMT-5 (Abcam ab246975, 1:1000).

After three 10-min TBST washes, membranes were incubated with HRP-conjugated goat anti-rabbit IgG secondary antibody (Abcam ab97051, 1:2000) for 1 h at room temperature. Protein bands were visualized using SuperSignal™ West Pico PLUS Chemiluminescent Substrate (Thermo Fisher, 34580). GAPDH (Abcam, ab9485 1:2000) served as loading control.

Chromatin immunoprecipitation (ChIP) assay

ChIP assays were performed using the EZ-ChIP Kit (Millipore, 17–371) according to the manufacturer's protocol. Briefly, 1×10^7 cells cultured in 6 cm dishes were cross-linked with 1% formaldehyde for 10 min at room temperature. The reaction was quenched with 125 mM glycine for 5 min. Cells were washed twice with ice-cold PBS containing protease inhibitor cocktail (Roche, 11873580001) and lysed in SDS lysis buffer (1% SDS, 10 mM EDTA, 50 mM Tris-HCl pH 8.1). Chromatin was sonicated to 200–500 bp fragments using a Bioruptor Pico (Diagenode) with 15 cycles of 30 s on/30 s off. Lysates were precleared with Protein G Sepharose beads (GE Healthcare, 17-0618-01) for 1 h at 4 °C. Immunoprecipitations were performed overnight at 4 °C with an anti-ATF1 antibody (Abcam, ab134104, 1:50) or normal rabbit IgG control (Abcam, ab313802). DNA-protein complexes were eluted using ChIP elution buffer (0.1 M NaHCO3, 1% SDS) and reverse cross-linked at 65 °C for 4 h. Purified DNA was analyzed by qPCR using SYBR Green Master Mix (Applied Biosystems, 4368577). Details of the primers utilized in this study can be found in Supplementary Table 1. Enrichment was calculated as % input using the formula: $2^{[(Ct(input) - Ct(ChIP)) \times 100]}$.

Statistics and reproducibility

All experiments were independently repeated at least three times using cells from a single isolation per experiment. Continuous variables are presented as mean ± standard deviation (SD). Comparisons between two groups were made using Student's t tests. All comparisons were predefined and hypothesis-driven. Given the limited number of independent tests per experiment, multiple comparison corrections were not applied to avoid overcorrection and loss of statistical power. Statistical analysis was performed using GraphPad Prism 7.0 (GraphPad Software, La Jolla, CA) or SPSS 22.0 (SPSS Inc., Chicago, IL). Significance levels were set at $^*P < 0.05$, $^{**}P < 0.01$, and $^{***}P < 0.001$.

Data availability

The raw transcriptomic data deposited in the GEO database (accession number: GSE15227). Uncropped and unedited blot/gel images are shown in Supplementary Figs. 1, 2 in the Supplementary Information PDF. The source data behind the graphs in the paper can be found in Supplementary Data Excel file. All other data are available from the corresponding author upon reasonable request.

Received: 4 October 2024; Accepted: 7 May 2025;
Published online: 14 May 2025

References

1. Kirnaz, S. et al. Fundamentals of intervertebral disc degeneration. *World Neurosurg.* **157**, 264–273 (2022).
2. Diseases, G. B. D. & Injuries, C. Global burden of 369 diseases and injuries in 204 countries and territories, 1990-2019: a systematic analysis for the Global Burden of Disease Study 2019. *Lancet* **396**, 1204–1222 (2020).
3. Adams, M. A. & Roughley, P. J. What is intervertebral disc degeneration, and what causes it?. *Spine* **31**, 2151–2161 (2006).
4. Wu, P. H., Kim, H. S. & Jang, I. T. Intervertebral disc diseases PART 2: a review of the current diagnostic and treatment strategies for intervertebral disc disease. *Int. J. Mol. Sci.* **21**, https://doi.org/10.3390/ijms21062135 (2020).
5. Xin, J. et al. Treatment of intervertebral disc degeneration. *Orthop. Surg.* **14**, 1271–1280 (2022).
6. Han, I. B. Moving forward: gene therapy for intervertebral disc degeneration. *Neurospine* **17**, 17–18 (2020).
7. Mok, G. F., Lozano-Velasco, E. & Munsterberg, A. microRNAs in skeletal muscle development. *Semin. Cell Dev. Biol.* **72**, 67–76 (2017).
8. Saliminejad, K., Khorram Khorshid, H. R., Soleymani Fard, S. & Ghaffari, S. H. An overview of microRNAs: biology, functions, therapeutics, and analysis methods. *J. Cell. Physiol.* **234**, 5451–5465 (2019).
9. Sun, W., Julie Li, Y. S., Huang, H. D., Shyy, J. Y. & Chien, S. microRNA: a master regulator of cellular processes for bioengineering systems. *Annu. Rev. Biomed. Eng.* **12**, 1–27 (2010).
10. Xiang, Q., Zhao, Y., Lin, J., Jiang, S. & Li, W. Epigenetic modifications in spinal ligament aging. *Ageing Res. Rev.* **77**, 101598 (2022).
11. Zhang, Y. et al. Dual functions of microRNA-17 in maintaining cartilage homeostasis and protection against osteoarthritis. *Nat. Commun.* **13**, 2447 (2022).
12. Wang, C. et al. The mechanism and function of miRNA in intervertebral disc degeneration. *Orthop. Surg.* **14**, 463–471 (2022).
13. Guo, W. et al. Circular RNA GRB10 as a competitive endogenous RNA regulating nucleus pulposus cells death in degenerative intervertebral disk. *Cell Death Dis.* **9**, 319 (2018).
14. Guo, W. et al. The circular RNA FAM169A functions as a competitive endogenous RNA and regulates intervertebral disc degeneration by targeting miR-583 and BTRC. *Cell Death Dis.* **11**, 315 (2020).
15. Ji, M. L. et al. Preclinical development of a microRNA-based therapy for intervertebral disc degeneration. *Nat. Commun.* **9**, 5051 (2018).
16. Mitchell, P. S. et al. Circulating microRNAs as stable blood-based markers for cancer detection. *Proc. Natl. Acad. Sci. USA* **105**, 10513–10518 (2008).
17. Silva, M. J. & Holguin, N. Aging aggravates intervertebral disc degeneration by regulating transcription factors toward chondrogenesis. *FASEB J.* **34**, 1970–1982 (2020).
18. He, R. et al. HIF1A Alleviates compression-induced apoptosis of nucleus pulposus derived stem cells via upregulating autophagy. *Autophagy* **17**, 3338–3360 (2021).

19. Hiyama, A., Mochida, J., Omi, H., Serigano, K. & Sakai, D. Cross talk between Smad transcription factors and TNF-alpha in intervertebral disc degeneration. *Biochem. Biophys. Res. Commun.* **369**, 679–685 (2008).
20. Wahid, F., Shehzad, A., Khan, T. & Kim, Y. Y. MicroRNAs: synthesis, mechanism, function, and recent clinical trials. *Biochim. Biophys. Acta* **1803**, 1231–1243 (2010).
21. Fazi, F. et al. A minicircuitry comprised of microRNA-223 and transcription factors NFI-A and C/EBPalpha regulates human granulopoiesis. *Cell* **123**, 819–831 (2005).
22. Davis, B. N. & Hata, A. Regulation of MicroRNA biogenesis: a miRiad of mechanisms. *Cell Commun. Signal.* **7**, 18 (2009).
23. Sylvestre, Y. et al. An E2F/miR-20a autoregulatory feedback loop. *J. Biol. Chem.* **282**, 2135–2143 (2007).
24. Liu, L. L. et al. ATF1/miR-214-5p/ITGA7 axis promotes osteoclastogenesis to alter OVX-induced bone absorption. *Mol. Med.* **28**, 56 (2022).
25. Liu, M. et al. Bioinformatics research and qRT-PCR verify hub genes and a transcription factor-microRNA feedback network in intervertebral disc degeneration. *Appl. Biochem. Biotechnol.* **196**, 3184–3198 (2024).
26. Luo, X., Wu, J. & Wu, G. PPARgamma activation suppresses the expression of MMP9 by downregulating NF-kappaB post intracerebral hemorrhage. *Neurosci. Lett.* **752**, 135770 (2021).
27. Lu, J. et al. Pseudolaric acid B ameliorates synovial inflammation and vessel formation by stabilizing PPARgamma to inhibit NF-kappaB signalling pathway. *J. Cell. Mol. Med.* **25**, 6664–6678 (2021).
28. Solleti, S. K. et al. Airway epithelial cell PPARgamma modulates cigarette smoke-induced chemokine expression and emphysema susceptibility in mice. *Am. J. Physiol. Lung Cell Mol. Physiol.* **309**, L293–L304 (2015).
29. Giridharan, S. & Srinivasan, M. Mechanisms of NF-κB p65 and strategies for therapeutic manipulation. *J. Inflamm. Res.* **11**, 407–419 (2018).
30. Cui, J. et al. Activating transcription factor 1 promoted migration and invasion in lung cancer cells through regulating EGFR and MMP-2. *Mol. Carcinog.* **58**, 1919–1924 (2019).
31. Li, T. et al. Phosphorylated ATF1 at Thr184 promotes metastasis and regulates MMP2 expression in gastric cancer. *J. Transl. Med.* **20**, 169 (2022).
32. Tong, Z., Cui, Q., Wang, J. & Zhou, Y. TransmiR v2.0: an updated transcription factor-microRNA regulation database. *Nucleic Acids Res.* **47**, D253–D258 (2019).
33. Zucman, J. et al. EWS and ATF-1 gene fusion induced by t(12;22) translocation in malignant melanoma of soft parts. *Nat. Genet.* **4**, 341–345 (1993).
34. Thomas, D. A. & Massague, J. TGF-beta directly targets cytotoxic T cell functions during tumor evasion of immune surveillance. *Cancer Cell* **8**, 369–380 (2005).
35. Cao, Y., Peng, Y. & Tang, Y. ATF1 regulates MAL2 expression through inhibition of miR-630 to mediate the EMT process that promotes cervical cancer cell development and metastasis. *J. Gynecol. Oncol.* https://doi.org/10.3802/jgo.2025.36.e11 (2024).
36. Henry, N., Clouet, J., Le Bideau, J., Le Visage, C. & Guicheux, J. Innovative strategies for intervertebral disc regenerative medicine: from cell therapies to multiscale delivery systems. *Biotechnol. Adv.* **36**, 281–294 (2018).
37. Clouet, J., Fusellier, M., Camus, A., Le Visage, C. & Guicheux, J. Intervertebral disc regeneration: from cell therapy to the development of novel bioinspired endogenous repair strategies. *Adv. Drug Deliv. Rev.* **146**, 306–324 (2019).
38. Yang, Z. et al. Novel role of the clustered miR-23b-3p and miR-27b-3p in enhanced expression of fibrosis-associated genes by targeting TGFBR3 in atrial fibroblasts. *J. Cell. Mol. Med.* **23**, 3246–3256 (2019).
39. Tavallaee, G. et al. Contribution of microRNA-27b-3p to synovial fibrotic responses in knee osteoarthritis. *Arthritis Rheumatol.* **74**, 1928–1942 (2022).
40. Agostini, M. et al. A pharmacogenetic approach to the treatment of patients with PPARG mutations. *Diabetes* **67**, 1086–1092 (2018).
41. Jabbari, P., Sadeghalvad, M. & Rezaei, N. An inflammatory triangle in Sarcoidosis: PPAR-gamma, immune microenvironment, and inflammation. *Expert Opin. Biol. Ther.* **21**, 1451–1459 (2021).
42. Hsieh, M. H. et al. Matrix metalloproteinase-1 polymorphism (-1607G) and disease severity in non-cystic fibrosis bronchiectasis in Taiwan. *PLoS ONE* **8**, e66265 (2013).
43. Liu, J., Zhao, N., Shi, G. & Wang, H. Geniposide ameliorated sepsis-induced acute kidney injury by activating PPARgamma. *Aging* **12**, 22744–22758 (2020).
44. Genovese, T. et al. Effect of rosiglitazone and 15-deoxy-Delta12,14-prostaglandin J2 on bleomycin-induced lung injury. *Eur. Respir. J.* **25**, 225–234 (2005).
45. Liu, X. et al. Sodium butyrate protects against oxidative stress in human nucleus pulposus cells via elevating PPARgamma-regulated Klotho expression. *Int. Immunopharmacol.* **85**, 106657 (2020).
46. Khasabova, I. A. et al. Pioglitazone, a PPARgamma agonist, reduces cisplatin-evoked neuropathic pain by protecting against oxidative stress. *Pain* **160**, 688–701 (2019).
47. Feng, C. et al. ROS: crucial intermediators in the pathogenesis of intervertebral disc degeneration. *Oxid. Med. Cell. Longev.* **2017**, 5601593 (2017).
48. Yao, M. et al. Marein protects human nucleus pulposus cells against high glucose-induced injury and extracellular matrix degradation at least partly by inhibition of ROS/NF-kappaB pathway. *Int Immunopharmacol.* **80**, 106126 (2020).
49. Jiang, Y., Dong, G. & Song, Y. Nucleus pulposus cell senescence is alleviated by resveratrol through regulating the ROS/NF-kappaB pathway under high-magnitude compression. *Biosci. Rep.* **38**, https://doi.org/10.1042/BSR20180670 (2018).
50. Jiang, H. et al. MicroRNA-338-3p as a novel therapeutic target for intervertebral disc degeneration. *Exp. Mol. Med.* **53**, 1356–1365 (2021).
51. Huan, T. et al. Genome-wide identification of microRNA expression quantitative trait loci. *Nat. Commun.* **6**, 6601 (2015).
52. Vautrot, V., Heckler, G., Aigueperse, C. & Behm-Ansmant, I. Fluorescence in situ hybridization of small non-coding RNAs. *Methods Mol. Biol.* **2300**, 73–85 (2021).

Acknowledgements

This study was supported by the Natural Science Foundation of Hebei (H2024110007), and the Natural Science Foundation of Cangzhou (221001009D).

Author contributions

Wei Guo designed the study and analysis. Experiments were performed by Wei Guo, Kun Mu, Jing-Chao Geng, Hai-Yang Xing, Yu Dong, Wen-Dong Liu, Jiao-Xiao Shi, Shuan-Chi Wang, and Bao-Rui Xing. Murine intervertebral discs were prepared by Hai-Yang Xing, Wen-Dong Liu, and Bao-Rui Xing. The study was supervised by Jian-Yong Zhao and Xiao-Ming Li. Wei Guo wrote the manuscript with contributions from Jing-Chao Geng. All the authors subsequently reviewed and edited the manuscript.

Competing interests

The authors declare no competing interests.

Additional information

Supplementary information The online version contains supplementary material available at https://doi.org/10.1038/s42003-025-08186-6.

Correspondence and requests for materials should be addressed to Wei Guo or Xiao-Ming Li.

Peer review information *Communications Biology* thanks Avijit Goswami and the other, anonymous, reviewer(s) for their contribution to the peer review of this work. Primary Handling Editors: Kaliya Georgieva.